1    Structurally conserved domains between flavivirus and alphavirus fusion glycoproteins

2    contribute to replication in mammals and infectious virion production.

3

4    Margarita V. Rangel[1], Nicholas Catanzaro[2], Sara A. Thannickal[1], Kelly A. Crotty[1], Maria G.

5    Noval[1], Katherine E.E. Johnson[3], Elodie Ghedin[3,4], Helen M. Lazear[2], and Kenneth A.

6    Stapleford[1,*]

7

8    [1]Department of Microbiology, New York University Grossman School of Medicine, New York ,

9    NY

10   [2]Department of Microbiology and Immunology, University of North Carolina at Chapel Hill,

11   Chapel Hill, NC

12   [3]Center for Genomics & Systems Biology, Department of Biology, New York University, New

13   York, NY.

14   [4]Systems Genomics Section, Laboratory of Parasitic Diseases, National Institute of Allergy and

15   Infectious Diseases, National Institute of Health, Bethesda, MD.

16

17

18

19

20   [*]Corresponding author: Kenneth Stapleford. Kenneth.stapleford@nyulangone.org

21

22

23   Short Title: Conserved mechanisms of class II fusion protein function.

24

25

26

**Abstract**

Alphaviruses and flaviviruses have class II fusion glycoproteins that are essential for virion assembly and infectivity. Importantly, the tip of domain II is structurally conserved between the alphavirus and flavivirus fusion proteins, yet whether these structural similarities between virus families translate to functional similarities is unclear. Using *in vivo* evolution of Zika virus (ZIKV), we identified several novel emerging variants including an envelope glycoprotein variant in β-strand c (V114M) of domain II. We have previously shown that the analogous β-strand c and the ij loop, located in the tip of domain II of the alphavirus E1 glycoprotein, are important for infectivity. This led us to hypothesize that flavivirus E β-strand c also contributes to flavivirus infection. We generated this ZIKV glycoprotein variant and found that while it had little impact on infection in mosquitoes, it reduced replication in human cells and mice, and increased virus sensitivity to ammonium chloride, as seen for alphaviruses. In light of these results and given our alphavirus ij loop studies, we mutated a conserved alanine at the tip of the flavivirus ij loop to valine to test its effect on ZIKV infectivity. Interestingly, this mutation inhibited infectious virion production of ZIKV and yellow fever virus, but not West Nile virus. Together, these studies show that structurally analogous residues in the alphavirus and flavivirus class II fusion proteins contribute to virus infection *in vivo* and highlight these shared domains as targets for broad-spectrum arbovirus therapies.

**Author Summary**

Arboviruses are a significant global public health threat, yet there are no antivirals targeting these viruses. This problem is in part due to our lack of knowledge on the molecular mechanisms involved in the arbovirus life cycle. In particular, virus entry and assembly are essential processes in the virus life cycle and steps that can be targeted for the development of antiviral therapies. Therefore, understanding common, fundamental mechanisms used by different arboviruses for entry and assembly is essential. In this study, we show that flavivirus and alphavirus residues located in structurally conserved and analogous regions of the class II fusion proteins contribute to common mechanisms of entry, dissemination, and infectious virion production. These studies highlight how class II fusion proteins function and provide novel targets for development of antivirals.

3

**Introduction**

63

64     Arthropod-borne viruses (arboviruses) are a diverse group of pathogens that can cause

65     explosive epidemics and devasting disease [1-4]. Arboviruses can be transmitted by a wide

66     variety of arthropod vectors including mosquitoes, ticks, and sandflies [5]. Importantly, vectors

67     such as *Aedes* (*Ae*.) species of mosquitoes can transmit several pathogenic arboviruses such

68     as dengue virus, Zika virus (ZIKV), and chikungunya virus (CHIKV), suggesting there may be

69     common mechanisms of infectivity shared among specific arboviruses. Currently there are

70     limited vaccines and no specific antiviral therapies targeting these viral threats, highlighting the

71     need to better understand at the molecular level how these viruses replicate and are

72     transmitted. In particular, identifying common mechanisms shared among arboviruses and

73     genetically distant arbovirus families could help determine broad-spectrum characteristics

74     needed for effective antivirals.

75     A common feature shared by all arboviruses is their need to be transmitted from an

76     insect vector to the human host, yet we understand little of the molecular mechanisms involved

77     in arbovirus transmission and infectivity. To study what contributes to arbovirus transmission we

78     can look at West Nile virus (WNV) [6, 7], ZIKV [8], Venezuelan equine encephalitis virus [9, 10],

79     and CHIKV [11]. Natural epidemics of these viruses have identified key residues in the viral

80     glycoproteins that promote virus transmission and infectivity. These findings along with years of

81     extensive experimentation have defined the viral glycoproteins as critical factors for virus

82     assembly, attachment and entry, transmission, and pathogenesis [12-18].

83     Alphaviruses and flaviviruses encode class II fusion proteins that are required for pH-

84     dependent entry and fusion [19, 20]. In a previous study, we used the *in vivo* evolution of CHIKV

85     during mosquito-to-mammal transmission to identify and study key determinants for alphavirus

86     infectivity and pathogenesis. In this study, we identified an adaptive variant (V80I) in β-strand c

87     of the E1 glycoprotein domain II which contributes to CHIKV transmission in mosquitos and

88     pathogenesis in mice [21]. In subsequent studies, we further characterized this residue and

89    found that V80 functions together with residue 226 on the ij loop of the tip of domain II to impact

90    pH- and cholesterol-dependent entry [22]. Importantly, the tip of domain II of the class II fusion

91    glycoprotein is structurally conserved between alphaviruses and flaviviruses. This observation

92    suggests that while these viruses are genetically unrelated, structural conservation in their

93    glycoproteins could translate to functional similarities between virus families.

94         In this study, we used *in vivo* evolution of ZIKV to identify factors involved in flavivirus

95    replication and infectivity. We identified novel variants in NS2A, NS3, and in β-strand c of

96    domain II of the ZIKV envelope protein. Given the structural similarities between domain II of the

97    alphavirus and flavivirus fusion glycoprotein, we hypothesized that β-strand c and the ij loop

98    may have analogous functions in both virus families. Here, we found that a highly conserved

99    valine in the ZIKV β-strand c attenuated virus replication in A549 cells and mice, and impacted

100    pH-dependent entry. Moreover, we found that analogous residues in the tip of the envelope ij

101    loop were important for ZIKV and yellow fever virus infectious virion production but not for WNV.

102    Together, these data provide functional evidence that alphaviruses and flaviviruses use similar

103    mechanisms and structural domains for infectivity and infectious virion production. These

104    studies further our understanding of arbovirus biology as well as open new avenues for the

105    development of antivirals targeting multiple virus families.

106

107

108

109

110

111

112

113

## Results

**Identification of emerging ZIKV variants in the envelope, NS2A, and NS3 during vector-borne transmission to type I interferon-deficient mice.** In a previous study to understand how transmission route and organ microenvironment impacts ZIKV evolution, we dissected the *in vivo* evolution of the prototype ZIKV strain (MR766) in type I interferon-deficient mice (*Ifnar1$^{-/-}$*) [23]. To do this, we infected *Ifnar1$^{-/-}$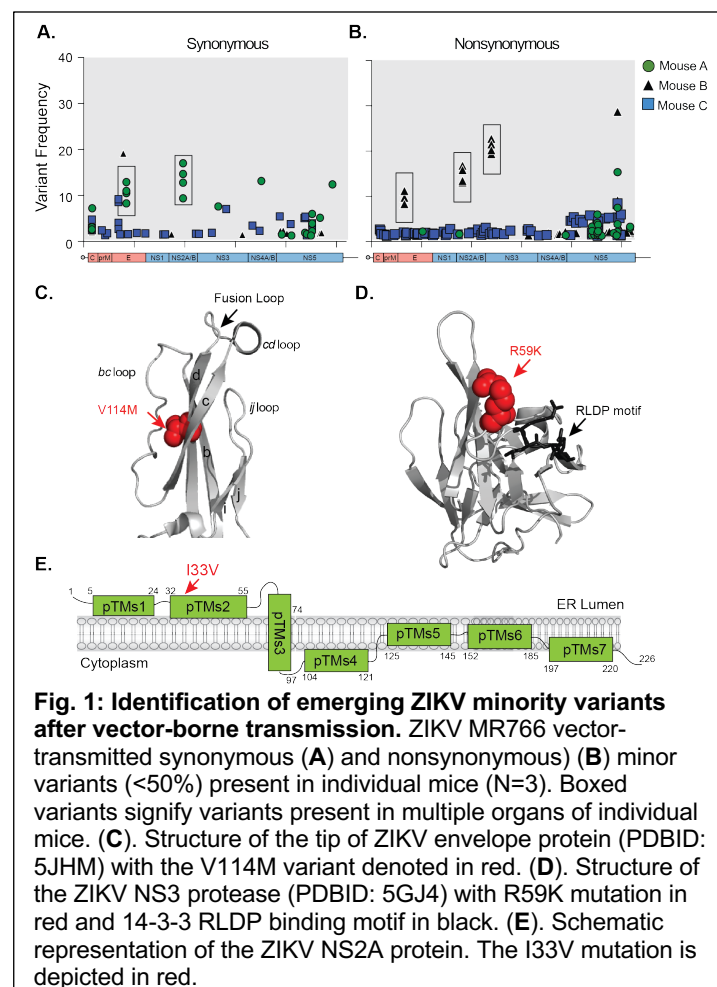* mice either by needle inoculation in the footpad or by mosquito bite from ZIKV infected *Ae. aegypti* mosquitoes, harvested organs at seven days post infection, and analyzed ZIKV variants by deep sequencing. Using the data from this study, we analyzed the synonymous a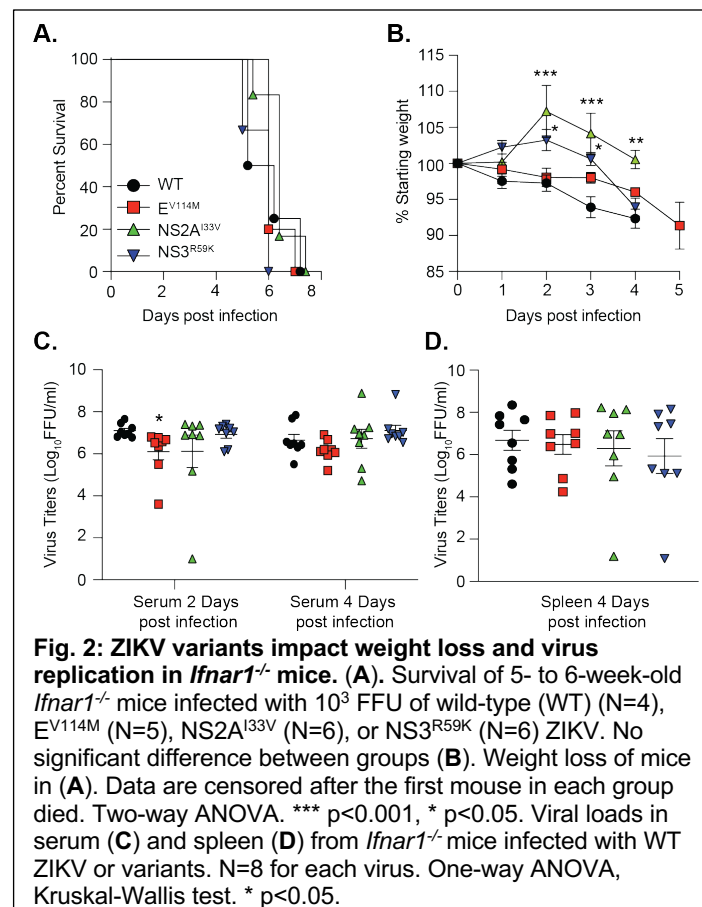nd nonsynonymous minority variants from mice after mosquito transmission (**Fig. 1**). We identified unique variants in two mice (Mouse A and Mouse B) that had the same point mutations in multiple organs (**Fig. 1A and B**, **boxes**). In Mouse A, there



**Fig. 1: Identification of emerging ZIKV minority variants after vector-borne transmission.** ZIKV MR766 vector-transmitted synonymous (**A**) and nonsynonymous) (**B**) minor variants (<50%) present in individual mice (N=3). Boxed variants signify variants present in multiple organs of individual mice. (**C**). Structure of the tip of ZIKV envelope protein (PDBID: 5JHM) with the V114M variant denoted in red. (**D**). Structure of the ZIKV NS3 protease (PDBID: 5GJ4) with R59K mutation in red and 14-3-3 RLDP binding motif in black. (**E**). Schematic representation of the ZIKV NS2A protein. The I33V mutation is depicted in red.
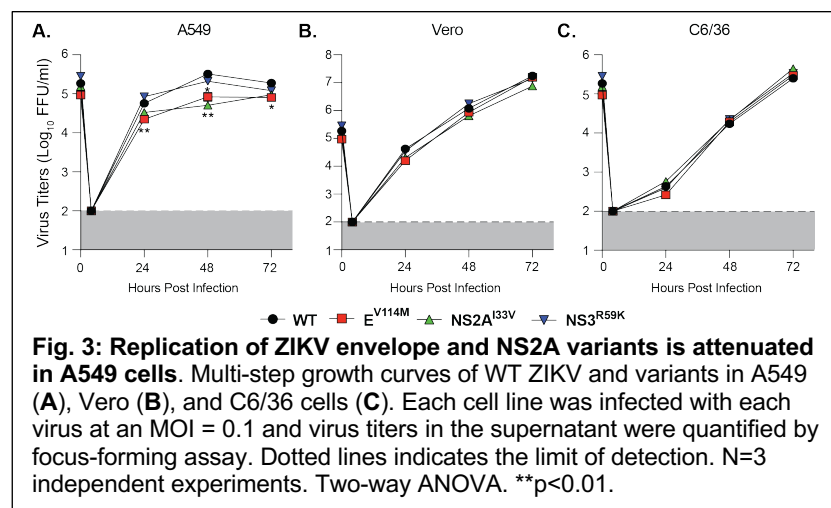
125    were two synonymous changes (C1690T (8.2-12.9%) and T3931C (9.4-17.0%)). In Mouse B,

126    there were three nonsynonymous changes (E: G1316A, V114M (8.9-9.2%); NS2A: A3638G,

127    I33V (13.1-16.8%); and NS3: G4788A, R59K (19.4-22.7%). When we mapped these changes

128    onto the protein structures we found that the $E^{V114M}$ mutation is located in the tip of domain II

129    which coincides with a highly conserved glycerophospholipid binding pocket [24] (**Fig. 1C**) and

130    the R59K mutation in NS3 maps near a cellular 14-3-3 binding site [25] (**Fig. 1D**). Finally, the

131    I33V mutation in NS2A is located in a putative transmembrane alpha-helix predicted to be in the

132    ER lumen [14] (**Fig. 1E**).

133

134    **ZIKV E, NS3, and NS2A variants have no significant advantage in *Ifnar1$^{-/-}$* mice and are**

135    **attenuated in A549 cells.** Given that these ZIKV variants were identified in *Ifnar1$^{-/-}$* mice*, we

136    tested whether this variant had a replication advantage in *Ifnar1$^{-/-}$* mice. We introduced each



**Fig. 2: ZIKV variants impact weight loss and virus replication in *Ifnar1$^{-/-}$* mice.** (**A**)**.** Survival of 5- to 6-week-old *Ifnar1$^{-/-}$* mice infected with $10^3$ FFU of wild-type (WT) (N=4), $E^{V114M}$ (N=5), NS2A$^{I33V}$ (N=6), or NS3$^{R59K}$ (N=6) ZIKV. No significant difference between groups (**B**). Weight loss of mice in (**A**). Data are censored after the first mouse in each group died. Two-way ANOVA. *** $p<0.001$, * $p<0.05$. Viral loads in serum (**C**) and spleen (**D**) from *Ifnar1$^{-/-}$* mice infected with WT ZIKV or variants. N=8 for each virus. One-way ANOVA, Kruskal-Wallis test. * $p<0.05$.
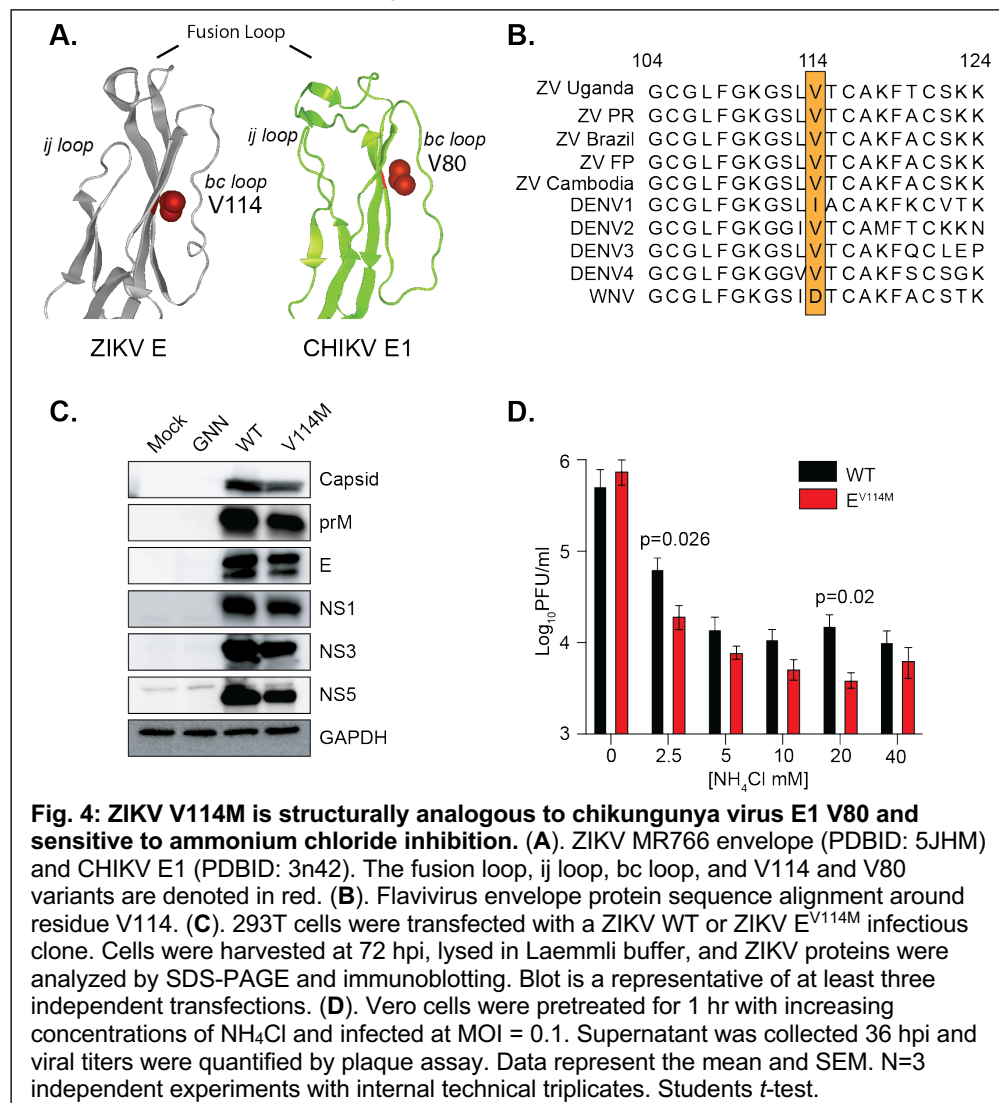
7

137    variant individually into an infectious clone of ZIKV strain MR766, infected *Ifnar1*^{-/-} mice with

138    each virus, and monitored survival and weight loss. All four viruses caused 100% lethality, with

139    no significant difference in the average time to death (**Fig. 2A**). Interestingly, we found that

140    although mice infected with each variant succumbed to infection at the same time as wild-type

141    (WT) ZIKV, the mice infected with the NS2A[I33V] and NS3[R59K] variants initially gained weight

142    followed by rapid weight loss and death (**Fig. 2B, green and purple triangles**). These data

143    suggest that NS2A and NS3 may play critical roles in ZIKV pathogenesis later in infection.

144         To investigate differences in viral replication between variants, we infected *Ifnar1*^{-/-} mice

145    with each variant and quantified infectious virus in the serum after 2- and 4-days post-infection,

146    and in the spleen at 4-days post infection (**Fig. 2C and D**). We found no significant advantage of

147    any of these variants in *Ifnar1*^{-/-} mice and, if anything, there was a reduction in replication

148    consistent with the weight loss results. Finally, to investigate the replication of each ZIKV variant

149    in cell culture, we performed multi-step growth curves in human A549, monkey Vero, and *Ae.*

150    *albopictus* C6/36 cells. We found that ZIKV E[V114M] and NS2A[I33V] were significantly attenuated in

151    A549 cells compared to WT virus (**Fig. 3A**), yet showed no differences in replication in Vero or

152    C6/36 cells (**Fig. 3C and D**). Together, these data indicate that these ZIKV variants show no

153    significant replication advantage in *Ifnar1*^{-/-} mice, yet are attenuated in IFN-competent human

154    cells, highlighting a role for these residues in ZIKV replication.



**Fig. 3: Replication of ZIKV envelope and NS2A variants is attenuated in A549 cells**. Multi-step growth curves of WT ZIKV and variants in A549 (**A**), Vero (**B**), and C6/36 cells (**C**). Each cell line was infected with each virus at an MOI = 0.1 and virus titers in the supernatant were quantified by focus-forming assay. Dotted lines indicates the limit of detection. N=3 independent experiments. Two-way ANOVA. **p<0.01.

155 **ZIKV E residue V114 is structurally analogous to alphavirus E1 residue V80 and is**

156 **important for pH-dependent entry.** We previously identified the CHIKV E1 glycoprotein

157 residue V80 in β-strand c as important for CHIKV pH-dependent entry [22]. Interestingly, the

158 ZIKV envelope residue V114 falls into a structurally analogous site in β-strand c of the ZIKV E

159 protein (**Fig. 4A**), and similar to alphaviruses [22], a valine at flavivirus residue 114 is highly

160 conserved (**Fig. 4B**). Given the similarities between ZIKV E$^{V114}$ and CHIKV E1$^{V80}$, we

161 hypothesized that ZIKV E$^{V114}$ may also contribute to ZIKV pH-dependent entry. To test this

162 hypothesis, we first tested that the ZIKV E$^{V114M}$ variant did not lead to any major differences in

163 viral protein accumulation or processing. To address this, we transfected 293T cells with
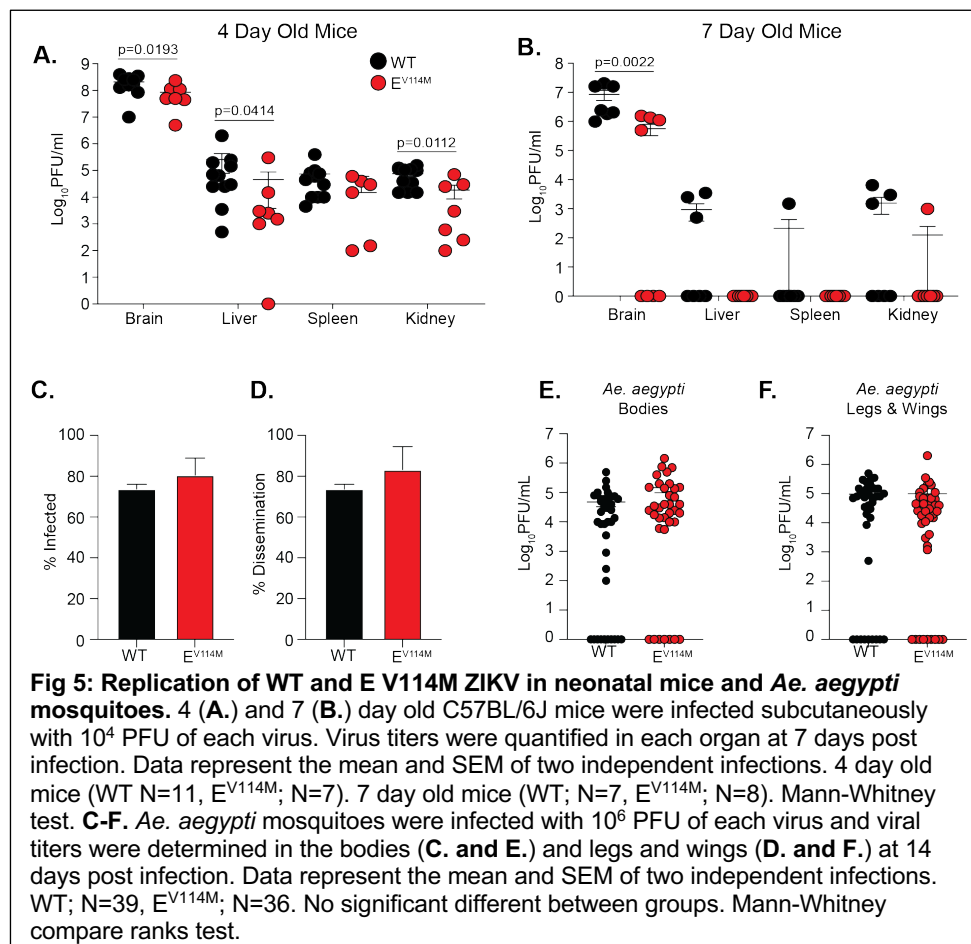


**Fig. 4: ZIKV V114M is structurally analogous to chikungunya virus E1 V80 and sensitive to ammonium chloride inhibition.** (**A**). ZIKV MR766 envelope (PDBID: 5JHM) and CHIKV E1 (PDBID: 3n42). The fusion loop, ij loop, bc loop, and V114 and V80 variants are denoted in red. (**B**). Flavivirus envelope protein sequence alignment around residue V114. (**C**). 293T cells were transfected with a ZIKV WT or ZIKV E$^{V114M}$ infectious clone. Cells were harvested at 72 hpi, lysed in Laemmli buffer, and ZIKV proteins were analyzed by SDS-PAGE and immunoblotting. Blot is a representative of at least three independent transfections. (**D**). Vero cells were pretreated for 1 hr with increasing concentrations of NH$_4$Cl and infected at MOI = 0.1. Supernatant was collected 36 hpi and viral titers were quantified by plaque assay. Data represent the mean and SEM. N=3 independent experiments with internal technical triplicates. Students $t$-test.

164   infectious clones encoding WT ZIKV, a replication-dead ZIKV harboring a mutation (GNN) in the

165   polymerase, or the E$^{V114M}$ variant.  We harvested cells at 72 hours post-transfection and

166   evaluated the accumulation of ZIKV proteins by western blot. While we found a slight reduction

167   in all proteins in the E$^{V114M}$ variant, possibly due to the replication defect in human cells, there

168   were no major differences in protein processing with the E$^{V114M}$ variant (**Fig. 4C**). Next, we asked

169   whether the ZIKV E$^{V114M}$ variant was sensitive to the lysosomotropic agent ammonium chloride

170   which will deacidify the endosome and block pH-dependent entry. We infected Vero cells with

171   each virus in the presence of increasing concentrations of ammonium chloride and found that

172   ZIKV E$^{V114M}$ replication was significantly more sensitive to the presence of ammonium chloride,

173   mimicking what we observed with CHIKV E1$^{V80}$ variants [22] (**Fig. 4D**). Together, these data

174   indicate that the flavivirus glycoprotein β-strand c contributes to pH-dependent entry as seen for
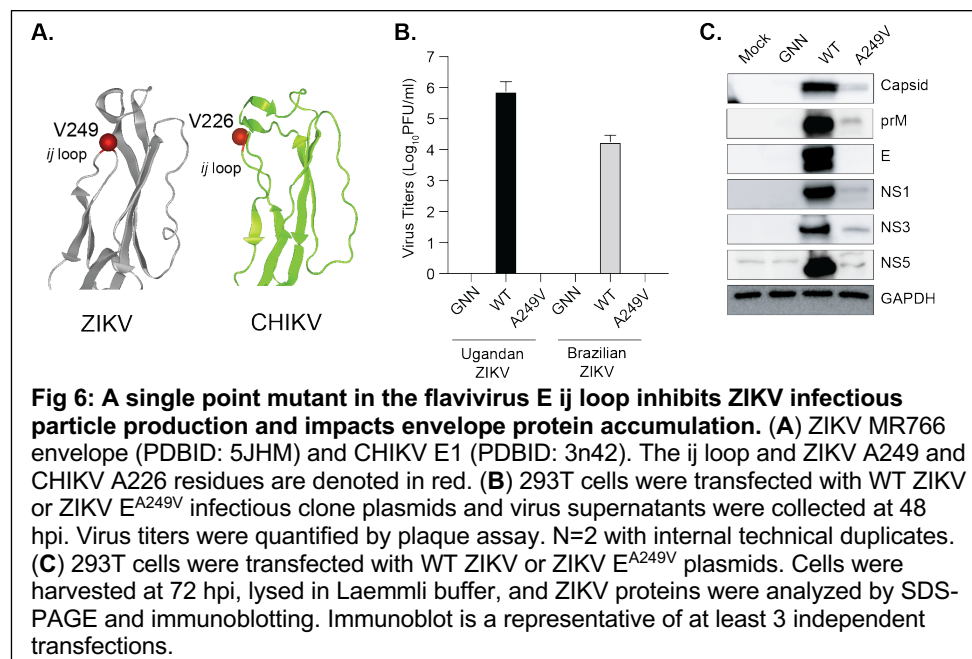
175   alphaviruses.

176

177   **ZIKV E$^{V114M}$ is attenuated in wild-type neonatal mice with no impact in replication in *Ae.***

178   ***aegypti* mosquitoes.** We observed that CHIKV E1$^{V80}$ contributes to dissemination in wild-type

179   mice and in *Ae. aegypti* mosquitoes [22]. Therefore, we hypothesized that ZIKV E$^{V114M}$ and ZIKV

180   envelope β-strand c may also play essential roles in dissemination in mice and mosquitoes. To

181   study ZIKV replication in WT immunocompetent mice, we first infected 6-week-old C57BL/6

182   mice; and as expected, neither virus replicated in these mice (data not shown). As an alternative

183   approach, we used 4- and 7-day old C57BL/6 neonatal mouse models. We hypothesized that

184   the 4-day old mice, which are more susceptible to ZIKV, would allow us to mimic the *Ifnar1$^{-/-}$*

185   mice while the 7-day old mice would allow us to study ZIKV infection in a model that is closer to

186   adult mice. We infected each neonatal model with WT ZIKV or the ZIKV E$^{V114M}$ variant. We

187   found that ZIKV E$^{V114M}$ was attenuated in its ability to replicate and disseminate in both 4- and 7-

188   day old mice (**Fig. 5A and B**). This attenuation of ZIKV E$^{V114M}$ was dependent on the age of the

10

189    mice as infection of the ZIKV $E^{V114M}$ variant was not detectable in the brain of several 7-day old

190    mice, suggesting that the virus may be cleared faster than WT ZIKV or there is a subset of 7-

191    day old mice that are specifically not susceptible to infection with the ZIKV $E^{V114M}$ variant.

192           To investigate how ZIKV $E^{V114M}$ impacts replication in mosquitoes, we infected *Ae.*

193    *aegypti* mosquitoes with WT ZIKV or the ZIKV $E^{V114M}$ variant and quantified viral titers in the

194    bodies, and legs and wings at 14 days post infection (**Fig. 5C-F**). We found no major difference

195    in the percentage of infected mosquitoes (**Fig. 5C**) or the percentage of mosquitoes that had

196    virus in the legs and wings (disseminated virus) (**Fig. 5D**). Interestingly, while we did not find a

197    statistically significant increase in viral titers with the ZIKV $E^{V114M}$ variant, the titers were higher

198    in multiple mosquitoes with no clear replication disadvantage (**Fig. E and F**). Together, these

199    data suggest that the flavivirus envelope β-strand c contributes to replication in neonatal mice

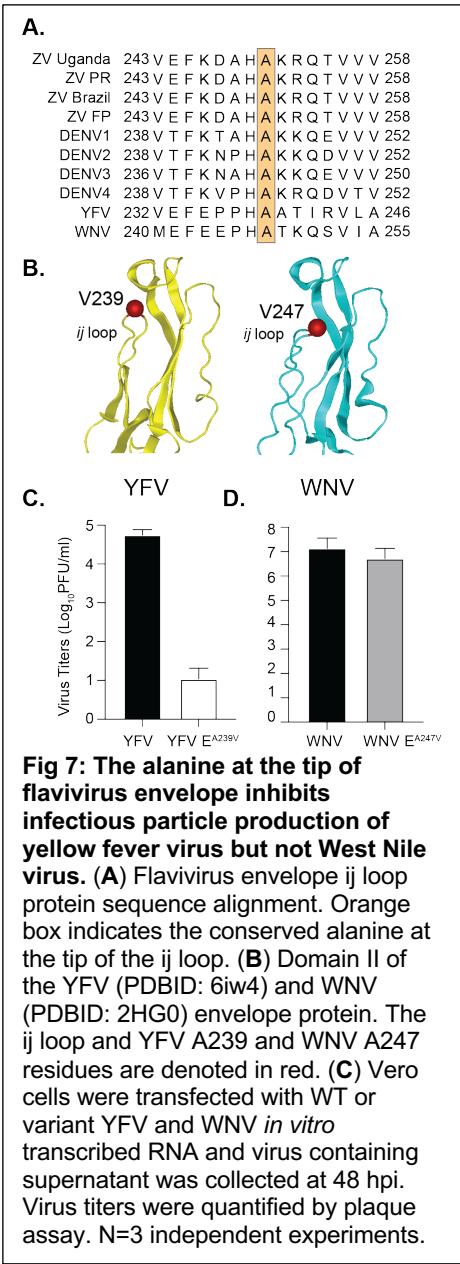200    with no negative impact on replication in mosquitoes.



**Fig 5: Replication of WT and E V114M ZIKV in neonatal mice and *Ae. aegypti* mosquitoes.** 4 (**A.**) and 7 (**B.**) day old C57BL/6J mice were infected subcutaneously with $10^4$ PFU of each virus. Virus titers were quantified in each organ at 7 days post infection. Data represent the mean and SEM of two independent infections. 4 day old mice (WT N=11, $E^{V114M}$; N=7). 7 day old mice (WT; N=7, $E^{V114M}$; N=8). Mann-Whitney test. **C-F.** *Ae. aegypti* mosquitoes were infected with $10^6$ PFU of each virus and viral titers were determined in the bodies (**C. and E.**) and legs and wings (**D. and F.**) at 14 days post infection. Data represent the mean and SEM of two independent infections. WT; N=39, $E^{V114M}$; N=36. No significant different between groups. Mann-Whitney compare ranks test.

201 **A conserved alanine at the tip of the flavivirus envelope protein ij loop is important for**

202 **ZIKV infectious particle production.** CHIKV has undergone several natural adaptation events

203 that have shaped its infectivity and transmission [26-28]. One of the most significant was the

204 emergence of a single amino acid substitution in the E1 glycoprotein (A226V) during an

205 epidemic on La Reunion Island [11]. This variant and residue 226, located in the ij loop of the

206 alphavirus E1 glycoprotein, has been shown to increase replication and transmission in *Ae.*

207 *albopictus* mosquitoes [27, 29] and is important for cholesterol-dependent entry [30,31].

208 Interestingly, flaviviruses contain a highly conserved alanine at the tip of the ij loop similar to

209 CHIKV (**Fig. 6A**). Given the structural similarities between the flavivirus and alphavirus class II

210 fusion proteins, we hypothesized that the ZIKV alanine would be important for virus infectivity.

211 We mutated this alanine (A249) to a valine in both the MR766 and Brazilian strains of ZIKV and

212 found that this single mutation completely blocked the production of infectious ZIKV particles in

213 293T cells as well as in BHK-21 and Vero cells (**Fig. 6B,** data not shown). One potential

214 explanation for this phenotype is that this mutation inhibits RNA replication and subsequent

215 protein production, as is the case for the NS5 GNN mutant (**Fig. 6**). To address whether ZIKV

216 E$^{A249V}$ impacted replication and/or protein production, we transfected 293T cells with each ZIKV



**Fig 6: A single point mutant in the flavivirus E ij loop inhibits ZIKV infectious particle production and impacts envelope protein accumulation. (A)** ZIKV MR766 envelope (PDBID: 5JHM) and CHIKV E1 (PDBID: 3n42). The ij loop and ZIKV A249 and CHIKV A226 residues are denoted in red. (**B**) 293T cells were transfected with WT ZIKV or ZIKV E$^{A249V}$ infectious clone plasmids and virus supernatants were collected at 48 hpi. Virus titers were quantified by plaque assay. N=2 with internal technical duplicates. (**C**) 293T cells were transfected with WT ZIKV or ZIKV E$^{A249V}$ plasmids. Cells were harvested at 72 hpi, lysed in Laemmli buffer, and ZIKV proteins were analyzed by SDS-PAGE and immunoblotting. Immunoblot is a representative of at least 3 independent transfections.

12

217    plasmids, harvested cells at 72 hours post-transfection, and analyzed protein accumulation by

218    western blotting. We detected the majority of ZIKV proteins in transfected cells, albeit at lower

219    levels due to the lack of spread of the ZIKV E$^{A249V}$ variant (**Fig. 6C**). Interestingly, the envelope

220    protein did not accumulate during transfection, suggesting that the virus is replicating yet may

221    not be producing infectious particles due to a defect in envelope accumulation (**Fig. 6C**). These

222    results indicate that the ZIKV ij loop is critical for infectious particle production potentially

223    through the stability of the envelope glycoprotein.

224

225    **Conserved alanine at the tip of flavivirus ij loop blocks YFV but not WNV infectious**

226    **particle production.** The alanine at the tip of the flavivirus ij loop is highly conserved among

227    flaviviruses and sits in the middle of a histidine and lysine which have been shown to be

228    important for virion assembly [32] (**Fig. 7A and B**). Given this conservation, we hypothesized

229    that the ij loop could also be critical for infectious particle production of other flaviviruses. To test

230    this hypothesis, we mutated the alanine at the tip of the E protein ij loop to a valine in the yellow

231    fever virus (YFV) and WNV infectious clones, transfected Vero cells with *in vitro* transcribed

232    RNA, and quantified infectious virions in the supernatant 48 hours later by plaque assay. We

233    found that the A-to-V mutation in YFV significantly impaired infectious virus production, while

234    this same mutation in WNV has no effect (**Fig. 7C and D**). Importantly, when we sequenced the

235    infectious virus from WNV, the A247V mutation was maintained and genetically stable. These

236    results indicate that the ij loop plays flavivirus-specific roles in virion assembly and the single

237    alanine at the tip of the ij loop contributes to infectious particle production. Future work will be

238    essential to understand how flavivirus and alphaviruses coordinate infections in insects and

239    mammals and to elucidate the differences in virus entry between flaviviruses.

**Fig 7: The alanine at the tip of flavivirus envelope inhibits infectious particle production of yellow fever virus but not West Nile virus.** (**A**) Flavivirus envelope ij loop protein sequence alignment. Orange box indicates the conserved alanine at the tip of the ij loop. (**B**) Domain II of the YFV (PDBID: 6iw4) and WNV (PDBID: 2HG0) envelope protein. The ij loop and YFV A239 and WNV A247 residues are denoted in red. (**C**) Vero cells were transfected with WT or variant YFV and WNV *in vitro* transcribed RNA and virus containing supernatant was collected at 48 hpi. Virus titers were quantified by plaque assay. N=3 independent experiments.

240

241

242

243

244

245

246

**Discussion**

248    Arboviruses are a diverse group of human pathogens belonging to multiple virus

249    families. There are no antiviral therapies targeting these viruses. This problem is in part due to

250    our incomplete understanding of the common, fundamental molecular mechanisms different

251    arboviruses use for infectivity and spread. To identify and study the fundamental mechanisms of

252    arbovirus biology, we use samples collected from natural infections and *in vivo* lab experiments.

253    In this study, we observed the emergence of ZIKV variants during vector-borne transmission

254    where three variants of interest were found in the E (V114M, ~10%), NS2A (I33V, ~15%), and

255    NS3 (R59K, ~20%) proteins. The envelope variant is located at the tip of the class II fusion

256    protein, near the fusion loop and the highly conserved glycerophospholipid-binding pocket [24].

257    The NS2A protein variant is located in a predicted alpha-helix near the ER membrane, and the

258    NS3 protease variant is close to an RLPD motif that was recently shown to be important for

259    interactions between NS3 and cellular 14-3-3 proteins to antagonize the innate immune

260    response [25]. Given that we originally found these variants in *Ifnar1$^{-/-}$* mice, we hypothesized

261    that they would play significant roles in ZIKV infection in mice. However, when in separate

262    experiments we introduced these variants into *Ifnar1$^{-/-}$* mice, they had no significant replication

263    advantage in the organs we investigated. These data and the fact that these variants were not

264    found in mice infected via needle inoculation [23], suggests that these variants may not have

265    been selected for in mice but rather in *Ae. aegypti* mosquitoes. This observation is particularly

266    interesting as the alphavirus glycoproteins have been highlighted many times in nature and in

267    the lab as a key evolutionary determinant for alphavirus infectivity and transmission in

268    mosquitoes [21, 26, 28]. This study provides evidence that this may also be the case for

269    flaviviruses as well. Importantly, future studies regarding the role of NS2A and NS3 in

270    mosquitoes and mice will be important to better understand the molecular mechanisms of the

271    flavivirus life cycle *in vivo*.

15

272     The ZIKV envelope has been shown to significantly contribute to virulence [8, 33-38].

273     The ZIKV envelope residue V114 is located in β-strand c of the glycoprotein domain II. Because

274     β-strand c of CHIKV plays an important role in virus dissemination and pathogenesis in mice

275     and transmission in mosquitoes, we hypothesize this would also be the case for flaviviruses.

276     Interestingly, we found that the ZIKV E$^{V114M}$ variant was attenuated in multiple mouse models

277     and in A549 cells, confirming that E residue V114 and β-strand c is important for flavivirus

278     infection. Given this attenuation in mammals, we thought that the ZIKV E$^{V114M}$ would have a

279     significant replication advantage in mosquitoes, yet while we did see an increased trend in

280     replication of the ZIKV E$^{V114M}$ variant in *Ae. aegypti* mosquitoes, this was not statistically

281     significant. One potential explanation for this could be that the E$^{V114M}$ mutation alone is not

282     enough to enhance replication and perhaps the combination of E, NS2A, and NS3 variants will

283     drive enhanced replication in mosquitoes and/or mice. Indeed, mutations in ZIKV NS3 have

284     been implicated in ZIKV infection in mice [39].  Moreover, as we only looked at one late time

285     point, it will be interesting to explore the temporal replication of these variants in mosquitoes and

286     mice to understand where the variants are acting during the viral life cycle. This is particularly

287     important for the NS2A and NS3 variants in mice, as we found that mice infected with these

288     variants gain weight in the beginning of the infection and rapidly succumb to the infection,

289     suggesting that NS2A and NS3 may play a role late in the infection.

290     In addition to the envelope domain II β-strand c, we also observed structural similarities

291     between the alphavirus and flavivirus glycoprotein ij loop. In CHIKV, a mutation from alanine to

292     valine at position 226, in the tip of the ij loop, was responsible for a significant outbreak that led

293     to increased replication in *Ae. albopictus* mosquitoes and to the emergence of the Indian Ocean

294     Lineage of CHIKV [11, 27]. However, when we made this same A-to-V mutation in ZIKV, there

295     was complete inhibition of infectious particle production, suggesting that the ij loop may play a

296     role in ZIKV particle assembly. This is plausible as previous work with Japanese encephalitis

16

297   virus (JEV) has shown that mutation of a conserved histidine and lysine in the ij loop impacts

298   JEV assembly [32]. In that study, the authors had hypothesized that these conserved charged

299   His and Lys residues in the envelope ij loop interact with negatively charged residues in prM to

300   promote assembly. This idea is intriguing. It is possible that the valine mutation in the ij loop also

301   destabilizes interactions between E and prM leading to reduction in infectious particle

302   production. However, this does not directly explain the specific reduction in the accumulation of

303   the $E^{A249V}$ protein in cells. Future studies will be important to understand how the ij loop

304   contributes to E stability and how the ij loop impacts ZIKV assembly.

305        Finally, we found that the alanine at the tip of the flavivirus ij loop behaves in a flavivirus

306   specific manner in that a mutation of alanine to valine in ZIKV and YFV blocked infectious virus

307   production, yet there was no such effect with WNV. In comparing the crystal structures of the

308   ZIKV, YFV, and WNV ij loop (**Fig. 7**) we noted that the alanine is oriented in a different direction

309   in WNV; and perhaps this change in structure is responsible for this phenotype. On the other

310   hand, there could be many other genetic differences between the envelope of ZIKV and WNV

311   that account for these differences in infectious particle production. Importantly, residue 114 in

312   ZIKV is a valine and in WNV 114 encodes for an aspartic acid, already suggesting differences in

313   E β-strand c function. This may help shed light on how flaviviruses such as ZIKV and WNV

314   infect different mosquito species and hosts such as birds.

315        Together, these studies have identified novel flavivirus variants that impact flavivirus

316   infection. We have shown that structurally similar domains of the flavivirus and alphavirus

317   envelope glycoproteins contribute to similar functions in virus infection. These common

318   mechanisms of infection could potentially provide the determinants needed for the development

319   of broad-spectrum antivirals. More importantly, these studies lead to new insight into the

320   fundamental biology of flaviviruses. Future studies to dissect the molecular details of the

321   flavivirus and alphavirus envelope proteins are critical to understand how these viruses function

322   and cause disease.

17

323 **Materials and Methods**

324 **Cells lines.**

325 293T cells (ATCC CRL3216) and Human Foreskin Fibroblasts (HFF1, ATCC SCRC-1041) were

326 grown in Dulbecco's Modified Eagle Medium (DMEM) supplemented with 1%

327 penicillin/streptomycin (P/S), 1% nonessential amino acids, and 10% heat-inactivated fetal

328 bovine serum (FBS, Atlanta Biologicals) at 37°C with 5% $CO_2$. Stapleford Lab Vero cells (ATCC

329 CCL-81) were maintained in DMEM supplemented with 1% P/S and 10% heat-inactivated

330 newborn calf serum (Gibco) at 37°C with 5% $CO_2$. Lazear Lab Vero and A549 cells were

331 maintained in DMEM containing 5% heat-inactivated FBS and L-glutamine at 37°C with 5%

332 $CO_2$. C6/36 cells were maintained in DMEM containing 6% FBS, NEAA, and P/S at 28°C with

333 5% $CO_2$. All cells were verified to be mycoplasma free.

334 **Viruses**

335 The ZIKV (Ugandan 1947 – MR766) wild-type and replication-deficient (NS5 GNN mutant)

336 plasmid infectious clones were a gift from Dr. Matthew Evans at the Icahn School of Medicine at

337 Mt. Sinai [40]. The ZIKV Brazilian strain infectious clone was a gift from Dr. Alexander Pletnev at

338 the National Institutes of Health [41]. The yellow fever virus (vaccine strain 17-D) infectious

339 clone was a gift from Dr. Julie Pfeiffer at the University of Texas Southwestern [42]. The West

340 Nile virus infectious clone was a gift from Dr. Gregory Ebel at Colorado State University [43].

341 The ZIKV, WNV, and YFV envelope variants were generated by site-directed mutagenesis

342 using Phusion high-fidelity polymerase (Thermo) and the primers in **Table 1**. All plasmids were

343 sequenced in full to confirm no second-site mutations were introduced.

**Table 1: Primers used for this study.**

| Virus and variant name | Sequence |
|---|---|
| MR766 ZIKV E V114M For | GGCAAAGGGAGCTTGATGACATGTGCCAAG |
| MR766 ZIKV E V114M For | CTTGGCACATGTCATCAAGCTCCCTTTGCC |
| MR766 ZIKV NS2A I21V For | GAGAATGACCACAAAGGTCATCATGAGCACATC |
| MR766 ZIKV NS2A I21V Rev | GATGTGCTCATGATGACCTTTGTGGTCATTCTC |
| MR766 ZIKV NS3 R42K For | CAAAAGGAGCCGCACTGAAGAGCGGTGAGGGAAGAC |
| MR766 ZIKV NS3 R42K Rev | GTCTTCCCTCACCGCTCTTCAGTGCGGCTCCTTTTG |
| MR766 ZIKV E A249V For | CAAGGATGCCCACGTCAAGAGGCAAACCG |

| MR766 ZIKV E A249V Rev | CGGTTTGCCTCTTGACGTGGGCATCCTTG |
|---|---|
| Brazilian ZIKV E A249V For | GTTCAAGGACGCACATGTCAAAAGGCAAACTGTCG |
| Brazilian ZIKV E A249V Rev | CGACAGTTTGCCTTTTGACATGTGCGTCCTTGAAC |
| YFV E A239V For | GAATTTGAACCTCCGCATGTCGCCACTATCAGAGTAC |
| YFV E A239V Rev | GTACTCTGATAGTGGCGACATGCGGAGGTTCAAATTC |
| WNV E A247V For | GTTTGAGGAACCACACGTCACGAAGCAGTCTGTG |
| WNV E A247V Rev | CACAGACTGCTTCGTGACGTGTGGTTCCTCAAAC |

344

345   The wild-type and variant Ugandan and Brazilian ZIKV were produced by transfecting

346 293T cells with 0.5 μg of each plasmid via Lipofectamine 2000 transfection reagent (Invitrogen).

347 Virus-containing supernatants were harvested 48 hrs post transfection, centrifuged at 1,200 x g

348 for 5 mins, aliquoted and stored at -80°C. To generate a working virus stock, Vero cells were

349 infected with transfection virus stocks and virus-containing supernatants were harvested 48 hrs

350 post infection, centrifuged at 1,200 x g for 5 mins, aliquoted, and stored at -80°C. Viral titers

351 were determined by plaque assay on Vero cells, as described below.

352   Wild-type and variant YFV and WNV were generated by the transfection of *in vitro*

353 transcribed RNA into Vero cells. In brief, YFV and WNV infectious clones were linearized

354 overnight with XhoI and XbaI respectively. Each plasmid was purified by phenol:chloroform

355 extraction and ethanol precipitation, resuspended in nuclease-free water. Linearized YFV and

356 WNV plasmids were used for in vitro transcription using the mMessage mMachine SP6 and T7

357 kits respectively following the manufacturer's instructions. In vitro transcribed RNAs were

358 purified by phenol:chloroform extraction and ethanol precipitation, diluted to 1 mg/ml, aliquoted

359 and stored at -80C. Vero cells (200,000 cells/well) were transfected with 5 μg of YFV and WNV

360 *in vitro* transcribed RNA via lipofectamine 2000 following the manufacturer's instructions and

361 incubated at 37°C for 48 hrs. Following incubation, virus titers were quantified by plaque assay

362 as described below. All work with WNV was performed under biosafety level 3 conditions.

363 **Deep sequencing analysis.** Sequencing data was published previously and can be found on

364 Sequence Read Archive (SRA) under BioProject ID PRJNA589089 [23]. Sequencing reads

365 were processed and aligned as described previously [23]. Minority variants were identified using

366 an in-house variant caller (https://github.com/GhedinLab/ZIKV_Analysis). Coverage and

367 minority variant calls were checked to ensure overlapping regions were identical in their

368 nucleotide composition before merging the fastq files and then realigning the 3 amplicons to the

369 reference file at once. Minority variants were called again on the merged alignment files and the

370 amino acid position was added using the positions indicated on the MR766 NCBI site

371 (KX830961.1). Minority variants were called if coverage at the given nucleotide was at or above

372 500x and the frequency of the variant was above 1%, present in both forward and reverse

373 reads, and had a quality score above 25.

374 **Plaque assay and focus-forming assay**

375 Viral titers were determined by plaque assay or focus-forming assay on Vero cells. For plaque

376 assays, virus was subjected to ten-fold serial dilutions in DMEM and added to a monolayer of

377 Vero cells for one hour at 37°C. Following incubation, a 0.8% agarose overlay was added, and

378 cells were incubated for five days at 37°C. Five days post infection, cells were fixed with 4%

379 formalin, the agarose overlay removed, and plaques were visualized by staining with crystal

380 violet (10% crystal violet and 20% ethanol). Viral titers were determined on the highest dilution

381 virus could be counted.

382  For focus-forming assays (FFA), duplicates of serial 10-fold dilutions of virus in viral

383 growth medium (DMEM containing 2% FBS and 20 mM HEPES) were applied to Vero cells in

384 96-well plates and incubated for 1 hr at 37°C. Following virus adsorption, the monolayers were

385 overlaid with 1% methylcellulose in minimum essential medium Eagle (MEM). Infected cell foci

386 were detected 42-46 hrs after infection. Following fixation with 2% paraformaldehyde (PFA) for

387 1 hr at room temperature, plates were incubated with 500 ng/ml of flavivirus cross-reactive

388 mouse MAb E60 [44] for 2 hr at room temperature or overnight at 4°C. After incubation at room

389 temperature for 2 hr with a 1:5,000 dilution of horseradish peroxidase (HRP)-conjugated goat

390 anti-mouse IgG (Sigma), foci were detected by addition of TrueBlue substrate (KPL). Foci were

391 quantified with a CTL Immunospot analyzer.

**Virus growth curves.**

For multi-step growth analysis, cells were infected at a multiplicity of infection of 0.1 and incubated at $37^{o}$C or $28^{o}$C with 5% $CO_2$ for one hour. Then, inoculum was aspirated and cells were washed with PBS and media was replenished. Samples of infected cell culture supernatant were collected at 4, 24, 48 and 72 hrs post-infection and stored at $-80^{o}$C for virus titration. Virus quantification was performed by FFA on Vero cells as above.

**Immunoblotting**

293T cells (500,000 cells/well in a 6-well plate) were transfected with 1.2 $\mu$g of each plasmid as described above. At predetermined time points, cells were harvested, washed twice with PBS, and resuspended in 2x Laemmli buffer containing 10% $\beta$-mercaptoethanol. Samples were boiled for 10 mins, centrifuged for 5 min at 12,000 x g to clarify debris, and proteins were separated by SDS-PAGE. Proteins were transferred to a PVDF membrane and membranes were blocked with 5% nonfat milk in Tris-buffered saline (TBS: 50 mM Tris pH 7.5, 150 mM NaCl) containing 0.1% Tween 20 (TBS-T). Membranes were incubated with anti-ZIKV capsid (Genetex; Cat #GTX133317), prM (Genetex; GTX133305), envelope (Genetex; Cat #GTX133314), NS1 (Genetex; Cat #GTX133307), NS3 and NS5 (gifts from Dr. Andres Merits at the University of Tartu, Estonia), and anti-GAPDH (GA1R ThermoFisher; Cat # MA5-15738) antibodies, washed with TBS-T and incubated with a horseradish peroxidase conjugated secondary antibody. After incubation with secondary antibody, membranes were washed extensively, developed with the SuperSignal West Pico chemiluminescent substrate (Pierce), and imaged on the BioRad Chemidoc imager. Images were analyzed and processed using ImageLab (Version 6.0.0).

**Mosquito infections and harvests**

*Ae. aegypti* mosquitoes (Poza Rica, Mexico, F30-35) were a gift from Dr. Gregory Ebel at Colorado State University [45]. Mosquitoes were reared and maintained in the NYU School of

21

417 Medicine ABSL3 facility at 28°C and 70% humidity with a 12:12 hour diurnal light cycle. The day

418 before infection, female mosquitoes were sorted and starved overnight. The day of infection,

419 mosquitoes were exposed to an infectious bloodmeal containing freshly washed sheep blood, 5

420 mM ATP, and $10^7$ PFU/ml virus. After approximately 30 mins, mosquitoes were cold-

421 anesthetized, and engorged female mosquitoes were sorted into new cups [46] [22]. Engorged

422 mosquitoes were incubated at 28°C with 70% humidity for 14 days and fed ad libitum with 10%

423 sucrose. Following incubation, mosquitoes were cold-anesthetized and the legs and wings

424 removed. Mosquito bodies and legs and wings were put into a 2 ml round-bottom tubes

425 containing 250 ml of PBS and a steel ball (Qiagen). Samples were homogenized using a

426 TissueLyser (Qiagen) with 30 shakes/second for 2 mins, centrifuged at 8,000 x g for 5 mins to

427 remove debris, and viral titers were quantified by plaque assay.

428 **Mouse infections**

429 4- and 7-day old WT C57BL/6J mouse experiments were completed in the NYU ABSL3 facility

430 performed under the approval of the NYU School of Medicine Institutional Animal Care and Use

431 Committee (IACUC) (Protocol # IA16-01783). 4- and 7-day old male and female C57BL/6J mice

432 were infected subcutaneously with $10^4$ PFU of the WT ZIKV or the ZIKV $E^{V114M}$ variant. Mice

433 were euthanized by decapitation seven dpi, organs harvested, homogenized as described

434 above, and ZIKV titers were quantified by plaque assay.

435 Husbandry and infections in type I Interferon-receptor knockout (*Ifnar1$^{-/-}$*) mice were

436 performed under the approval of the University of North Carolina at Chapel Hill IACUC (Protocol

437 # 19-185). 5- to 6-week-old male *Ifnar1$^{-/-}$* mice on a C57BL/6 background were used. Mice were

438 inoculated with $10^3$ FFU of ZIKV in a volume of 50 $\mu$l by a subcutaneous route in the footpad.

439 Survival and weight loss were monitored for 14 days. Animals that lost ≥30% of their starting

440 weight or that exhibited severe disease signs were euthanized by isoflurane overdose. Weights

441 are reported as percent of weight at the day of infection and group means were censored once

442 one animal in a group died. To measure viral loads, ZIKV-infected mice were euthanized at 4 dpi

22

443     as above and perfused with 20 ml of PBS. Spleens were harvested and homogenized with

444     zirconia beads (BioSpec) in a MagNA Lyser instrument (Roche Life Science) in 1 ml of PBS.

445     Blood was collected at 2 dpi by submandibular bleed with a 5 mm Goldenrod lancet and by cardiac

446     puncture at 4 dpi. Blood was collected in serum separator tubes (BD) and serum was separated

447     by centrifugation at 8000 rpm for 5 min. Tissues and serum from infected animals were stored at

448     -80$^{\circ}$C until titration by focus-forming assay.

449     **Virus protein accession numbers**

450     GenBank accession numbers used for flavivirus protein alignments: Zika MR766 (KX830960.1),

451     ZIKV Puerto Rican (KX377337), ZIKV Brazilian (KX280026.1), ZIKV French Polynesia

452     (KJ776791.2), ZIKV Cambodian (KU955593.1), DENV1 (BCG29749), DENV2 (BCG29762),

453     DENV3 (AVF19960), DENV4 (BCG29769), YFV (NP_740305), and WNV (MN849176).

454     **Protein structures**

455     The E glycoprotein structure of ZIKV (PDB: 5JHM), WNV (PDB: 2HG0), YFV (PDB: 6iw4), and

456     the CHIKV E1 glycoprotein structure (PDB: 3n4) were visualized using Protein 3D

457     (www.dnastar.com).

458     **Statistical analysis**

459     GraphPad Prism (Version 8.0.2) was used to analyze all data and perform statistical analyses.

460     All *in vitro* experiments were completed in triplicate with internal duplicates or triplicates.

461     Mosquito and mouse experiments were completed in two independent infection. $p < 0.05$ is

462     considered significant.

463

464     **Acknowledgements**

473

**References**

475     1.      Coffey LL, Forrester N, Tsetsarkin K, Vasilakis N, Weaver SC. Factors shaping the

476     adaptive landscape for arboviruses: implications for the emergence of disease. Future Microbiol.

477     2013;8(2):155-76. doi: 10.2217/fmb.12.139. PubMed PMID: 23374123; PubMed Central

478     PMCID: PMCPMC3621119.

479     2.      Weaver SC, Reisen WK. Present and future arboviral threats. Antiviral Res.

480     2010;85(2):328-45. doi: 10.1016/j.antiviral.2009.10.008. PubMed PMID: 19857523; PubMed

481     Central PMCID: PMCPMC2815176.

482     3.      Weaver SC, Charlier C, Vasilakis N, Lecuit M. Zika, Chikungunya, and Other Emerging

483     Vector-Borne Viral Diseases. Annu Rev Med. 2018;69:395-408. Epub 2017/08/29. doi:

484     10.1146/annurev-med-050715-105122. PubMed PMID: 28846489; PubMed Central PMCID:

485     PMCPMC6343128.

486     4.      Pierson TC, Diamond MS. The continued threat of emerging flaviviruses. Nat Microbiol.

487     2020;5(6):796-812. Epub 2020/05/06. doi: 10.1038/s41564-020-0714-0. PubMed PMID:

488     32367055; PubMed Central PMCID: PMCPMC7696730.

489     5.      Kramer LD. Complexity of virus-vector interactions. Curr Opin Virol. 2016;21:81-6. doi:

490     10.1016/j.coviro.2016.08.008. PubMed PMID: 27580489; PubMed Central PMCID:

491     PMCPMC5138088.

492     6.      Brault AC, Huang CY, Langevin SA, Kinney RM, Bowen RA, Ramey WN, et al. A single

493     positively selected West Nile viral mutation confers increased virogenesis in American crows.

494     Nat Genet. 2007;39(9):1162-6. doi: 10.1038/ng2097. PubMed PMID: 17694056; PubMed

495     Central PMCID: PMCPMC2291521.

496     7.      Ebel GD, Carricaburu J, Young D, Bernard KA, Kramer LD. Genetic and phenotypic

497     variation of West Nile virus in New York, 2000-2003. Am J Trop Med Hyg. 2004;71(4):493-500.

498     PubMed PMID: 15516648.

499     8.      Shan C, Xia H, Haller SL, Azar SR, Liu Y, Liu J, et al. A Zika virus envelope mutation

500     preceding the 2015 epidemic enhances virulence and fitness for transmission. Proc Natl Acad

501     Sci U S A. 2020;117(33):20190-7. Epub 2020/08/05. doi: 10.1073/pnas.2005722117. PubMed

502     PMID: 32747564; PubMed Central PMCID: PMCPMC7443865.

503     9.      Brault AC, Powers AM, Ortiz D, Estrada-Franco JG, Navarro-Lopez R, Weaver SC.

504     Venezuelan equine encephalitis emergence: enhanced vector infection from a single amino acid

505     substitution in the envelope glycoprotein. Proc Natl Acad Sci U S A. 2004;101(31):11344-9. doi:

506     10.1073/pnas.0402905101. PubMed PMID: 15277679; PubMed Central PMCID:

507     PMCPMC509205.

508     10.     Brault AC, Powers AM, Holmes EC, Woelk CH, Weaver SC. Positively charged amino

509     acid substitutions in the e2 envelope glycoprotein are associated with the emergence of

510     venezuelan equine encephalitis virus. J Virol. 2002;76(4):1718-30. PubMed PMID: 11799167;

511     PubMed Central PMCID: PMCPMC135911.

512     11.     Schuffenecker I, Iteman I, Michault A, Murri S, Frangeul L, Vaney MC, et al. Genome

513     microevolution of chikungunya viruses causing the Indian Ocean outbreak. PLoS Med.

514     2006;3(7):e263. doi: 10.1371/journal.pmed.0030263. PubMed PMID: 16700631; PubMed

515     Central PMCID: PMCPMC1463904.

516     12.     Jose J, Snyder JE, Kuhn RJ. A structural and functional perspective of alphavirus

517     replication and assembly. Future Microbiol. 2009;4(7):837-56. Epub 2009/09/03. doi:

518     10.2217/fmb.09.59. PubMed PMID: 19722838; PubMed Central PMCID: PMCPMC2762864.

519    13.    Nicholls CMR, Sevvana M, Kuhn RJ. Structure-guided paradigm shifts in flavivirus

520    assembly and maturation mechanisms. Adv Virus Res. 2020;108:33-83. Epub 2020/01/01. doi:

521    10.1016/bs.aivir.2020.08.003. PubMed PMID: 33837721; PubMed Central PMCID:

522    PMCPMC7510438.

523    14.    Barnard TR, Abram QH, Lin QF, Wang AB, Sagan SM. Molecular Determinants of

524    Flavivirus Virion Assembly. Trends Biochem Sci. 2021;46(5):378-90. Epub 2021/01/12. doi:

525    10.1016/j.tibs.2020.12.007. PubMed PMID: 33423940.

526    15.    Carro SD, Cherry S. Beyond the Surface: Endocytosis of Mosquito-Borne Flaviviruses.

527    Viruses. 2020;13(1). Epub 2020/12/31. doi: 10.3390/v13010013. PubMed PMID: 33374822;

528    PubMed Central PMCID: PMCPMC7824540.

529    16.    Brown RS, Wan JJ, Kielian M. The Alphavirus Exit Pathway: What We Know and What

530    We Wish We Knew. Viruses. 2018;10(2). Epub 2018/02/23. doi: 10.3390/v10020089. PubMed

531    PMID: 29470397; PubMed Central PMCID: PMCPMC5850396.

532    17.    Button JM, Qazi SA, Wang JC, Mukhopadhyay S. Revisiting an old friend: new findings

533    in alphavirus structure and assembly. Curr Opin Virol. 2020;45:25-33. Epub 2020/07/20. doi:

534    10.1016/j.coviro.2020.06.005. PubMed PMID: 32683295; PubMed Central PMCID:

535    PMCPMC7746636.

536    18.    Holmes AC, Basore K, Fremont DH, Diamond MS. A molecular understanding of

537    alphavirus entry. PLoS Pathog. 2020;16(10):e1008876. Epub 2020/10/23. doi:

538    10.1371/journal.ppat.1008876. PubMed PMID: 33091085; PubMed Central PMCID:

539    PMCPMC7580943 on the Scientific Advisory Board of Moderna. The Diamond laboratory has

540    received unrelated funding under sponsored research agreements from Vir Biotechnology,

541    Moderna, and Emergent BioSolutions.

542    19.    Vaney MC, Rey FA. Class II enveloped viruses. Cell Microbiol. 2011;13(10):1451-9.

543    Epub 2011/07/28. doi: 10.1111/j.1462-5822.2011.01653.x. PubMed PMID: 21790946.

544    20.    Kielian M. Class II virus membrane fusion proteins. Virology. 2006;344(1):38-47. Epub

545    2005/12/21. doi: 10.1016/j.virol.2005.09.036. PubMed PMID: 16364734.

546    21.    Stapleford KA, Coffey LL, Lay S, Borderia AV, Duong V, Isakov O, et al. Emergence and

547    transmission of arbovirus evolutionary intermediates with epidemic potential. Cell Host Microbe.

548    2014;15(6):706-16. doi: 10.1016/j.chom.2014.05.008. PubMed PMID: 24922573.

549    22.    Noval MG, Rodriguez-Rodriguez BA, Rangel MV, Stapleford KA. Evolution-Driven

550    Attenuation of Alphaviruses Highlights Key Glycoprotein Determinants Regulating Viral

551    Infectivity and Dissemination. Cell Rep. 2019;28(2):460-71 e5. Epub 2019/07/11. doi:

552    10.1016/j.celrep.2019.06.022. PubMed PMID: 31291581.

553    23.    Johnson KEE, Noval MG, Rangel MV, De Jesus E, Geber A, Schuster S, et al. Mapping

554    the evolutionary landscape of Zika virus infection in immunocompromised mice. Virus Evol.

555    2020;6(2):veaa092. Epub 2021/01/08. doi: 10.1093/ve/veaa092. PubMed PMID: 33408879;

556    PubMed Central PMCID: PMCPMC7772475.

557    24.    Guardado-Calvo P, Atkovska K, Jeffers SA, Grau N, Backovic M, Perez-Vargas J, et al.

558    A glycerophospholipid-specific pocket in the RVFV class II fusion protein drives target

559    membrane insertion. Science. 2017;358(6363):663-7. doi: 10.1126/science.aal2712. PubMed

560    PMID: 29097548.

561    25.    Riedl W, Acharya D, Lee JH, Liu G, Serman T, Chiang C, et al. Zika Virus NS3 Mimics a

562    Cellular 14-3-3-Binding Motif to Antagonize RIG-I- and MDA5-Mediated Innate Immunity. Cell

563    Host Microbe. 2019;26(4):493-503 e6. Epub 2019/10/11. doi: 10.1016/j.chom.2019.09.012.

564    PubMed PMID: 31600501; PubMed Central PMCID: PMCPMC6922055.

565    26.    Tsetsarkin KA, Chen R, Sherman MB, Weaver SC. Chikungunya virus: evolution and

566    genetic determinants of emergence. Curr Opin Virol. 2011;1(4):310-7. doi:

567    10.1016/j.coviro.2011.07.004. PubMed PMID: 21966353; PubMed Central PMCID:

568    PMCPMC3182774.

569    27.    Tsetsarkin KA, Vanlandingham DL, McGee CE, Higgs S. A single mutation in

570    chikungunya virus affects vector specificity and epidemic potential. PLoS Pathog.

571    2007;3(12):e201. doi: 10.1371/journal.ppat.0030201. PubMed PMID: 18069894; PubMed

572    Central PMCID: PMCPMC2134949.

573    28.    Tsetsarkin KA, Chen R, Leal G, Forrester N, Higgs S, Huang J, et al. Chikungunya virus

574    emergence is constrained in Asia by lineage-specific adaptive landscapes. Proc Natl Acad Sci U

575    S A. 2011;108(19):7872-7. doi: 10.1073/pnas.1018344108. PubMed PMID: 21518887; PubMed

576    Central PMCID: PMCPMC3093459.

577    29.    Arias-Goeta C, Moutailler S, Mousson L, Zouache K, Thiberge JM, Caro V, et al.

578    Chikungunya virus adaptation to a mosquito vector correlates with only few point mutations in

579    the viral envelope glycoprotein. Infect Genet Evol. 2014;24:116-26. doi:

580    10.1016/j.meegid.2014.03.015. PubMed PMID: 24681263.

581    30.    Tsetsarkin KA, McGee CE, Higgs S. Chikungunya virus adaptation to Aedes albopictus

582    mosquitoes does not correlate with acquisition of cholesterol dependence or decreased pH

583    threshold for fusion reaction. Virol J. 2011;8:376. doi: 10.1186/1743-422X-8-376. PubMed

584    PMID: 21801412; PubMed Central PMCID: PMCPMC3162544.

585    31.    Vashishtha M, Phalen T, Marquardt MT, Ryu JS, Ng AC, Kielian M. A single point

586    mutation controls the cholesterol dependence of Semliki Forest virus entry and exit. J Cell Biol.

587    1998;140(1):91-9. Epub 1998/02/14. doi: 10.1083/jcb.140.1.91. PubMed PMID: 9425157;

588    PubMed Central PMCID: PMCPMC2132589.

589    32.    Liu H, Liu Y, Wang S, Zhang Y, Zu X, Zhou Z, et al. Structure-based mutational analysis

590    of several sites in the E protein: implications for understanding the entry mechanism of

591    Japanese encephalitis virus. J Virol. 2015;89(10):5668-86. Epub 2015/03/13. doi:

592    10.1128/JVI.00293-15. PubMed PMID: 25762738; PubMed Central PMCID: PMCPMC4442514.

593    33.    Bos S, Viranaicken W, Frumence E, Li G, Despres P, Zhao RY, et al. The Envelope

594    Residues E152/156/158 of Zika Virus Influence the Early Stages of Virus Infection in Human

595   Cells. Cells. 2019;8(11). Epub 2019/11/17. doi: 10.3390/cells8111444. PubMed PMID:

596   31731738; PubMed Central PMCID: PMCPMC6912530.

597   34.    Giraldo MI, Xia H, Aguilera-Aguirre L, Hage A, van Tol S, Shan C, et al. Envelope

598   protein ubiquitination drives entry and pathogenesis of Zika virus. Nature. 2020;585(7825):414-

599   9. Epub 2020/07/10. doi: 10.1038/s41586-020-2457-8. PubMed PMID: 32641828; PubMed

600   Central PMCID: PMCPMC7501154.

601   35.    Duggal NK, McDonald EM, Weger-Lucarelli J, Hawks SA, Ritter JM, Romo H, et al.

602   Mutations present in a low-passage Zika virus isolate result in attenuated pathogenesis in mice.

603   Virology. 2019;530:19-26. Epub 2019/02/15. doi: 10.1016/j.virol.2019.02.004. PubMed PMID:

604   30763872; PubMed Central PMCID: PMCPMC6441372.

605   36.    Carbaugh DL, Baric RS, Lazear HM. Envelope Protein Glycosylation Mediates Zika

606   Virus Pathogenesis. J Virol. 2019;93(12). Epub 2019/04/05. doi: 10.1128/JVI.00113-19.

607   PubMed PMID: 30944176; PubMed Central PMCID: PMCPMC6613755.

608   37.    Carbaugh DL, Lazear HM. Flavivirus Envelope Protein Glycosylation: Impacts on Viral

609   Infection and Pathogenesis. J Virol. 2020;94(11). Epub 2020/03/13. doi: 10.1128/JVI.00104-20.

610   PubMed PMID: 32161171; PubMed Central PMCID: PMCPMC7269438.

611   38.    Carbaugh DL, Zhou S, Sanders W, Moorman NJ, Swanstrom R, Lazear HM. Two

612   Genetic Differences between Closely Related Zika Virus Strains Determine Pathogenic

613   Outcome in Mice. J Virol. 2020;94(20). Epub 2020/08/17. doi: 10.1128/JVI.00618-20. PubMed

614   PMID: 32796074; PubMed Central PMCID: PMCPMC7527068.

615   39.    Collette NM, Lao VHI, Weilhammer DR, Zingg B, Cohen SD, Hwang M, et al. Single

616   Amino Acid Mutations Affect Zika Virus Replication In Vitro and Virulence In Vivo. Viruses.

617   2020;12(11). Epub 2020/11/18. doi: 10.3390/v12111295. PubMed PMID: 33198111; PubMed

618   Central PMCID: PMCPMC7697975.

619   40.    Schwarz MC, Sourisseau M, Espino MM, Gray ES, Chambers MT, Tortorella D, et al.

620   Rescue of the 1947 Zika Virus Prototype Strain with a Cytomegalovirus Promoter-Driven cDNA

621   Clone. mSphere. 2016;1(5). Epub 2016/10/06. doi: 10.1128/mSphere.00246-16. PubMed PMID:

622   27704051; PubMed Central PMCID: PMCPMC5040786.

623   41.     Tsetsarkin KA, Kenney H, Chen R, Liu G, Manukyan H, Whitehead SS, et al. A Full-

624   Length Infectious cDNA Clone of Zika Virus from the 2015 Epidemic in Brazil as a Genetic

625   Platform for Studies of Virus-Host Interactions and Vaccine Development. MBio. 2016;7(4). doi:

626   10.1128/mBio.01114-16. PubMed PMID: 27555311; PubMed Central PMCID:

627   PMCPMC4999549.

628   42.     Erickson AK, Pfeiffer JK. Dynamic viral dissemination in mice infected with yellow fever

629   virus strain 17D. J Virol. 2013;87(22):12392-7. Epub 2013/09/13. doi: 10.1128/JVI.02149-13.

630   PubMed PMID: 24027319; PubMed Central PMCID: PMCPMC3807901.

631   43.     Grubaugh ND, Fauver JR, Ruckert C, Weger-Lucarelli J, Garcia-Luna S, Murrieta RA, et

632   al. Mosquitoes Transmit Unique West Nile Virus Populations during Each Feeding Episode. Cell

633   Rep. 2017;19(4):709-18. doi: 10.1016/j.celrep.2017.03.076. PubMed PMID: 28445723.

634   44.     Oliphant T, Nybakken GE, Engle M, Xu Q, Nelson CA, Sukupolvi-Petty S, et al. Antibody

635   recognition and neutralization determinants on domains I and II of West Nile Virus envelope

636   protein. J Virol. 2006;80(24):12149-59. Epub 2006/10/13. doi: 10.1128/JVI.01732-06. PubMed

637   PMID: 17035317; PubMed Central PMCID: PMCPMC1676294.

638   45.     Ruckert C, Weger-Lucarelli J, Garcia-Luna SM, Young MC, Byas AD, Murrieta RA, et al.

639   Impact of simultaneous exposure to arboviruses on infection and transmission by Aedes aegypti

640   mosquitoes. Nat Commun. 2017;8:15412. doi: 10.1038/ncomms15412. PubMed PMID:

641   28524874.

642   46.     Kaczmarek ME, Herzog NL, Noval MG, Zuzworsky J, Shah Z, Bajwa WI, et al. Distinct

643   New York City Aedes albopictus Mosquito Populations Display Differences in Salivary Gland

644   Protein D7 Diversity and Chikungunya Virus Replication. Viruses. 2020;12(7). Epub 2020/07/02.

645   doi: 10.3390/v12070698. PubMed PMID: 32605312; PubMed Central PMCID:

646   PMCPMC7411853.

647 **Figure Legends**

648 **Fig. 1: Identification of emerging ZIKV minority variants after vector-borne transmission.**

649 ZIKV MR766 vector-transmitted synonymous (**A**) and nonsynonymous) (**B**) minor variants

650 (<50%) present in individual mice (N=3). Boxed variants signify variants present in multiple

651 organs of individual mice. (**C**). Structure of the tip of ZIKV envelope protein (PDBID: 5JHM) with

652 the V114M variant denoted in red. (**D**). Structure of the ZIKV NS3 protease (PDBID: 5GJ4) with

653 R59K mutation in red and 14-3-3 RLDP binding motif in black. (**E**). Schematic representation of

654 the ZIKV NS2A protein. The I33V mutation is depicted in red.

655

656 **Fig. 2: ZIKV variants impact weight loss and virus replication in *Ifnar1*$^{-/-}$ mice. (A).** Survival

657 of 5- to 6-week-old *Ifnar1*$^{-/-}$ mice infected with $10^3$ FFU of wild-type (WT) (N=4), E$^{V114M}$ (N=5),

658 NS2A$^{I33V}$ (N=6), or NS3$^{R59K}$ (N=6) ZIKV. No significant difference between groups (**B**). Weight

659 loss of mice in (**A**). Data are censored after the first mouse in each group died. Two-way

660 ANOVA. *** $p<0.001$, * $p<0.05$. Viral loads in serum (**C**) and spleen (**D**) from *Ifnar1*$^{-/-}$ mice

661 infected with WT ZIKV or variants. N=8 for each virus. One-way ANOVA, Kruskal-Wallis test. *

662 $p<0.05$.

663

664 **Fig. 3: Replication of ZIKV envelope and NS2A variants is attenuated in A549 cells**. Multi-

665 step growth curves of WT ZIKV and variants in A549 (**A**), Vero (**B**), and C6/36 cells (**C**). Each

666 cell line was infected with each virus at an MOI = 0.1 and virus titers in the supernatant were

667 quantified by focus-forming assay. Dotted lines indicates the limit of detection. N=3 independent

668 experiments. Two-way ANOVA. ** $p<0.01$.

669

670 **Fig. 4: ZIKV V114M is structurally analogous to chikungunya virus E1 V80 and sensitive**

671 **to ammonium chloride inhibition. (A).** ZIKV MR766 envelope (PDBID: 5JHM) and CHIKV E1

672 (PDBID: 3n42). The fusion loop, ij loop, bc loop, and V114 and V80 variants are denoted in red.

31

673     (**B**). Flavivirus envelope protein sequence alignment around residue V114. (**C**). 293T cells were

674     transfected with a ZIKV WT or ZIKV $E^{V114M}$ infectious clone. Cells were harvested at 72 hpi,

675     lysed in Laemmli buffer, and ZIKV proteins were analyzed by SDS-PAGE and immunoblotting.

676     Blot is a representative of at least three independent transfections. (**D**). Vero cells were

677     pretreated for 1 hr with increasing concentrations of $NH_4Cl$ and infected at MOI = 0.1.

678     Supernatant was collected 36 hpi and viral titers were quantified by plaque assay. Data

679     represent three independent experiments with internal technical triplicates. Data represent the

680     mean and SEM. Students t-test.

681

682     **Fig 5: Replication of WT and E V114M ZIKV in neonatal mice and *Ae. aegypti* mosquitoes.**

683     4 (**A.**) and 7 (**B.**) day old C57BL/6J mice were infected subcutaneously with $10^4$ PFU of each

684     virus. Virus titers were quantified in each organ at 7 days post infection. Data represent the

685     mean and SEM of two independent infections. 4 day old mice (WT N=11, $E^{V114M}$; N=7). 7 day

686     old mice (WT; N=7, $E^{V114M}$; N=8). Mann-Whitney test. **C-F.** *Ae. aegypti* mosquitoes were

687     infected with $10^6$ PFU of each virus and viral titers were determined in the bodies (**C. and E.**)

688     and legs and wings (**D. and F.**) at 14 days post infection. Data represent the mean and SEM of

689     two independent infections. WT; N=39, $E^{V114M}$; N=36. No significant different between groups.

690     Mann-Whitney compare ranks test.

691

692     **Fig 6: A single point mutant in the flavivirus E ij loop inhibits ZIKV infectious particle**

693     **production and impacts envelope protein accumulation.** (**A**) ZIKV MR766 envelope

694     (PDBID: 5JHM) and CHIKV E1 (PDBID: 3n42). The ij loop and ZIKV A249 and CHIKV A226

695     residues are denoted in red. (**B**) 293T cells were transfected with WT ZIKV or ZIKV $E^{A249V}$

696     infectious clone plasmids and virus supernatants were collected at 48 hpi. Virus titers were

697     quantified by plaque assay. N=2 with internal technical duplicates. (**C**) 293T cells were

698     transfected with WT ZIKV or ZIKV $E^{A249V}$ plasmids. Cells were harvested at 72 hpi, lysed in

699    Laemmli buffer, and ZIKV proteins were analyzed by SDS-PAGE and immunoblotting.

700    Immunoblot is a representative of at least 3 independent transfections.

701

702    **Fig 7: The alanine at the tip of flavivirus envelope inhibits infectious particle production**

703    **of yellow fever virus but not West Nile virus.** (**A**) Flavivirus envelope ij loop protein sequence

704    alignment. Orange box indicates the conserved alanine at the tip of the ij loop. (**B**) Domain II of

705    the YFV (PDBID: 6iw4) and WNV (PDBID: 2HG0) envelope protein. The ij loop and YFV A239

706    and WNV A247 residues are denoted in red. (**C**) Vero cells were transfected with WT or variant

707    YFV and WNV *in vitro* transcribed RNA and virus containing supernatant was collected at 48

708    hpi. Virus titers were quantified by plaque assay. N=3 independent experiments.

709